Probing atomic environments in alloys by electron spectroscopy

T. L. Underwood, G. J. Ackland, and R. J. Cole
School of Physics and Astronomy, SUPA, The University of Edinburgh, Edinburgh, EH9 3JZ, United Kingdom
(Received 11 February 2014; revised manuscript received 17 June 2014; published 8 July 2014)

In alloys exhibiting substitutional disorder, the variety of atomic environments manifests itself as a "disorder broadening" in their core-level binding-energy spectra. Disorder broadening can be measured experimentally and, in principle, can be used to deduce information about specific atomic environments within a sample. However, progress in this endeavor is hampered by the lack of a model for this phenomenon which can treat complex systems. In this work we describe such a model. The model is used to elucidate the relationship between charge transfer, atomic environment, and disorder broadening in complex systems, with a focus on the problem of characterizing the interface quality of CuNi multilayers. We also validate the model against the results of *ab initio* electronic-structure calculations. Several counterintuitive aspects of the disorder-broadening phenomenon are uncovered, an understanding of which is essential for the correct interpretation of experimental results. For instance, it is shown that systems with inhomogeneous concentration profiles can exhibit disorder broadenings significantly larger than random alloys. Furthermore, in some systems a "disorder narrowing" is even possible.

DOI: 10.1103/PhysRevB.90.014201 PACS number(s): 79.60.Ht, 71.23.−k, 79.60.Jv

I. INTRODUCTION

An atom's core-level binding energies depend on its chemical species. This fact has been exploited for decades in order to determine the proportion of different species within a given sample via core-level spectroscopy, which provides the distribution of core-electron binding energies within a sample. An atom's binding energies also depend on its environment, i.e., the species of its surrounding atoms. For instance, in a Cu metal all atoms have the same environment, and hence the binding energies for a given Cu core-level type, e.g., $2p_{3/2}$, will be the same for all atoms. By contrast, in a CuPd alloy exhibiting substitutional disorder, the Cu atoms exhibit a variety of environments, and hence also a variety of $2p_{3/2}$ binding energies. Such a dispersion in the binding energies has been observed in many alloy systems [1–8] and in theory can be used to deduce information about specific environments within a sample, including the concentration profile on the atomic scale. The viability of achieving this via high-kinetic-energy photoelectron spectroscopy (HIKE) has recently been demonstrated [7,8]. This is promising because HIKE, unlike other widely used techniques, is both bulk sensitive and nondestructive. Such environment-resolved spectroscopy would prove useful to the many research areas involving alloys in which segregation plays a crucial role, e.g., metal embrittlement [9–14] and nanocatalyst design [15,16]. However, success in this endeavor hinges upon a solid understanding of the relationship between an atom's environment, its electronic structure, and its core-level binding energies in alloys.

The central quantity with regards to environment-resolved spectroscopy in alloys is the (alloy-metal) core-level shift (CLS), which for a core level bound to an X site i is defined as

$$\Delta E_i^{\mathrm{B}} = E_i^{\mathrm{B}} - E_{X\mathrm{met}}^{\mathrm{B}}, \tag{1}$$

where E_i^{B} is the binding energy of the core level, and $E_{X\mathrm{met}}^{\mathrm{B}}$ is the binding energy of the core level belonging to the type under consideration in a pure X metal. Note that this is a site-dependent quantity: one must determine ΔE_i^{B} for all X sites in the system under consideration in order to determine the X CLS distribution. This is problematic for systems exhibiting substitutional disorder on account of their lack of periodicity, which is a prerequisite for treatment within the conventional theoretical framework exploited by most *ab initio* methods. One way around this problem is to approximate the system under consideration as periodic, but with a large unit cell, i.e., a supercell. In this *supercell approximation* one determines ΔE_i^{B} for all X sites and hopes that the range of environments exhibited by these sites is representative of the "true" (nonperiodic) system and hence will result in an accurate representation of the true X CLS distribution.

Random alloys—the archetype of disordered alloys in which there are no correlations between the species of sites—are the most tractable system exhibiting substitutional disorder to treat theoretically and have been the focus of both experimental [1–6,17] and theoretical [1,2,6,17–23] attempts to understand the distribution of CLSs in alloys. In this context the dispersion of X CLSs is known as "disorder broadening" on account of the increased width of, for example, the Cu CLS distribution for a CuPd random alloy relative to that for a Cu metal. Sophisticated *ab initio* models utilizing the supercell approximation have provided insight into disorder broadening in these systems [6,17,22,23]. However, most systems of practical interest cannot be idealized as random alloys, and unfortunately the complexity of these systems is such that a description of their disorder broadenings using *ab initio* models is intractable within the supercell approximation.

Accurate methods do exist which do not resort to the supercell approximation. *Ab initio* methods rooted in the coherent potential approximation (CPA) [24–26] have been shown to provide excellent agreement with experiment [17,27–30]. Furthermore, they can treat complex systems [7,17,30]. However, CPA-based approaches cannot provide detailed information regarding the disorder broadening in complex systems—nor even in random alloys. While phenomenological models have been developed which can provide such information [1,2,18,19,21], their accuracy has been questioned [31–33]. One criticism is that these models do not take into account "final-state effects" associated with changes in the valence-electron density after photoemission. It

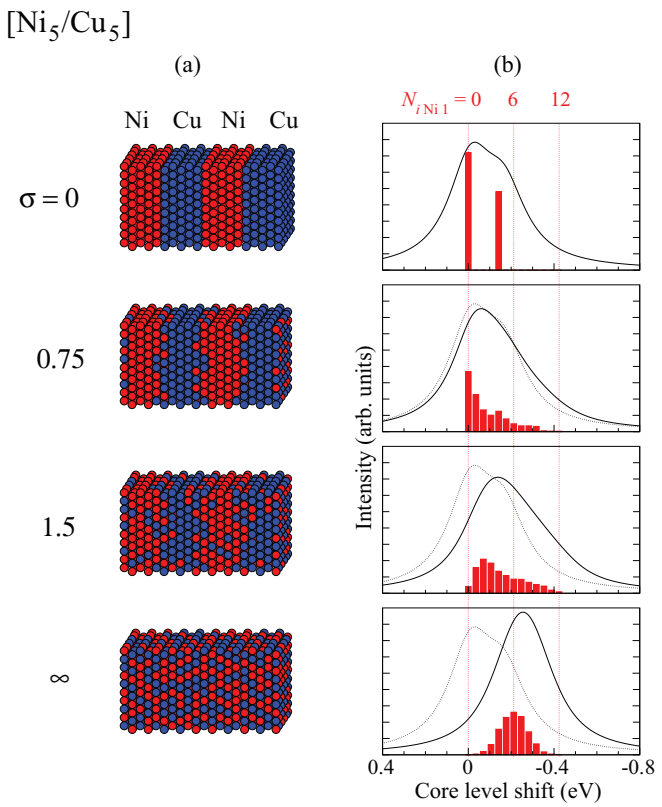

FIG. 1. (Color online) (a) Schematic illustration of $[Ni_5/Cu_5]$ at various σ, and (b) the corresponding model spectra. In panel (b), each red bar corresponds to a different value of N_{iNi1}: the ordinate of the bar is the CLS corresponding to N_{iNi1} according to Eq. (69), and its height reflects the frequency of Cu sites with that value of N_{iNi1}. The bars corresponding to $N_{iNi1} = 0$, 6, and 12 are indicated. The dotted curves in panel (b) are spectra for $\sigma = 0$.

has even been claimed that the complexity of the relationship between CLSs and environment in alloys precludes an accurate alternative to *ab initio* methods [33].

Here we present an accurate phenomenological model for CLSs in alloys which relates ΔE_i^B—including the final state contribution—to the environment of site i. The model, like previous approaches, is charge-transfer based and provides a simple framework for rationalizing the disorder-broadening phenomenon. The layout of this work is as follows: In Sec. II we review the theory which underpins the model and derive expressions for CLSs which apply to a wide range of alloy systems. We then apply the model to the problem of characterizing the interface quality of metallic multilayers. This problem has received significant attention on account of its importance to nanotechnology [7,8,17,34] and can be restated as follows: what is the degree of "interface roughening" σ in a given sample? Figure 1(a) provides an illustration of the multilayer system $[Ni_5/Cu_5]$ with various σ—where the square brackets signify that the system at $\sigma = 0$ consists of a ten-monolayer stack Ni_5/Cu_5 repeated throughout all space. In this regard, Sec. III contains details of our calculations, and our results are presented in Sec. IV. Finally, in Sec. V we summarize our main findings and discuss the limitations of the model and intentions for future work. Note that, throughout this work, we use Hartree atomic units unless otherwise stated. To transform energies within Hartree atomic units to eV the former quantity should be multiplied by a factor 27.2114.

II. THEORY

Our model is based on the charge-excess functional model [35] within the nonrandom approximation [21,36] (NRA-CEFM). After briefly reviewing the NRA-CEFM in Sec. II A, in Sec. II B we use it to derive a relation between ΔE_i^B and the environment of site i. In the subsequent sections this relation is itself used to derive expressions for the mean and full width at half maximum (FWHM) of various CLS distributions. While our expression for ΔE_i^B presented in Sec. II B is valid for *any* alloy—subject to the assumptions which underpin the NRA-CEFM—our expressions for means and FWHMs apply only to the class of alloys which can be described as having a concentration profile which varies along one direction from monolayer to monolayer. To elaborate, for an alloy belonging to this class, the quantities c_X^l for all X and l describe the concentration profile, where c_X^l denotes the concentration of X sites within monolayer l, and we are assuming that the species of sites belonging to a given monolayer l are assigned randomly in the appropriate concentrations. Note that this class includes random alloys, for which $c_X^l = c_X$ for all l, where c_X denotes the global concentration of species X. Furthermore, note that we use the following convention for labeling the monolayers: monolayer l is the lth monolayer in the direction in which the concentrations of each species are varying.

A. Charge-excess functional model in nonrandom approximation

The charge-excess functional model (CEFM) [35] has been shown to provide an accurate description of the charge distribution in disordered alloys [35–37]. It has also been shown to provide an accurate description of energy differences between alloy configurations with the same *composition* [37]—where by composition we mean a specification of the underlying lattice and the quantities c_X for all X. In the CEFM the alloy energy is postulated to take the form

$$E = E_0 + \frac{1}{2}\sum_i a_i (Q_i - b_i)^2 + E_M, \tag{2}$$

where

$$E_M = \frac{1}{2}\sum_i Q_i V_i \tag{3}$$

is the Madelung energy, V_i is the Madelung potential of site i, Q_i is the net charge on site i, a_i is the strength of the "local interactions" within site i which act to keep the charge of site i at its "bare" value b_i, and E_0 is a constant. For all X sites, a_i and b_i take the same values a_X and b_X, respectively. Minimizing E subject to the constraint of charge neutrality leads to the following expression [35]:

$$V_i = -a_i Q_i + k_i, \tag{4}$$

where

$$k_i = a_i b_i + \lambda, \tag{5}$$

and λ is a Lagrange multiplier added to enforce charge neutrality. Equation (4) describes the Q-V relations, which are borne out in *ab initio* calculations to a high degree of accuracy [37–40]. This partly explains the success of the CEFM.

Equation (2) can be derived within the class of generalized coherent potential approximations (GCPAs) described by Bruno *et al.* [37], with the additional—essentially exact [37]—assumption that charge transfer due to Madelung interactions [48] is small. Here we consider the CEFM within this framework, in which case b_X is equivalent to the charge of an X site embedded in the GCPA effective medium for the system under consideration, given the constraint that the site's Madelung potential is zero. In other words, b_X is the charge of an X site embedded in the effective medium if the Madelung interactions are "switched off." Furthermore, a_X is the linear response coefficient relating the Madelung potential of the X site to its perturbation from b_X, and E_0 is the energy of the alloy if the Madelung interactions between sites are switched off, which can be expressed as

$$E_0 = \mathcal{N} \sum_X c_X \mathcal{E}_X, \tag{6}$$

where $\mathcal{E}_X$ is the energy of an X site embedded in the effective medium if Madelung interactions are switched off, and $\mathcal{N}$ is the total number of sites in the system. Conventional CPA calculations do not take into account Madelung interactions, and hence for GCPA theories based upon CPA effective media, b_X is simply the charge of an X site obtained from a conventional CPA calculation, and $\mathcal{E}_X$ is the corresponding X energy. Calculations reveal that GCPA effective media are numerically indistinguishable [37] for all alloys with the same composition. Hence the same applies for the quantities b_X, a_X, and E_0: these quantities are transferable between such systems.

The complexity of the CEFM is significantly reduced if one makes the assumption that a_X takes the same value a for all species [21,36,41]. This assumption is known as the nonrandom approximation (NRA), and we use it throughout this work. The nonrandom approximation is borne out by calculations utilizing the single-site locally self-consistent Green's function method [40]—a GCPA method. In the NRA-CEFM Q_i for an X site obeys [21]

$$Q_i = \Lambda \sum_Y b_{YX} \sum_{\beta=1}^{\infty} g_\beta N_{iY\beta}, \tag{7}$$

where $N_{iY\beta}$ is the number of Y sites in the βth nearest-neighbor shell of site i,

$$b_{YX} \equiv (b_Y - b_X), \tag{8}$$

and the quantities Λ and g_β for all β depend only on $a R_{\mathrm{WS}}$ and the underlying lattice *type* [49] where R_{WS} is the Wigner–Seitz radius for the system under consideration—and are tabulated in Ref. [21] for the fcc, bcc, and sc lattices. Note that the free parameters a and b_{YX} (for all X,Y) can be obtained from *ab initio* calculations or by other means [21]. Furthermore, the values of $N_{iY\beta}$ for all β and Y characterize the environment of i. Therefore Eq. (7) explicitly relates Q_i to the environment of site i. Equation (7) also allows us to interpret an alloy's charge distribution in terms of charge transfer between pairs of *unlike* sites as follows [21]: an X site gains a charge $\Lambda b_{YX} g_\beta$ from each Y site in its βth nearest-neighbor shell, with the Y site losing the opposite amount. This picture allows us to attribute the following physical significance to the quantity b_Y: it is a measure of the *electropositivity* of species Y for the given composition.

B. Expression for ΔE_i^{B}

We will now use the NRA-CEFM to derive an expression for the CLS of site i. To do this, we first derive an expression for the total energy E in terms of the bare charges b_i of all sites. Equation (2) can be rewritten more explicitly as

$$E = E_0 + \frac{1}{2} a \sum_i (Q_i - b_i)^2 + \frac{1}{2} \sum_i Q_i V_i \tag{9}$$

for the NRA-CEFM, where we have used Eq. (3). Minimizing this with respect to the site charges and subject to the constraint of global charge neutrality gives [21]

$$V_i = -a Q_i + a (b_i - \langle b \rangle), \tag{10}$$

where $\langle b \rangle$ denotes the mean value of b_i over all i. Substituting the above into Eq. (9) and simplifying gives

$$E = \frac{1}{2} a \sum_i \left(b_i^2 - b_i Q_i \right) + E_0, \tag{11}$$

where we have used the fact that

$$\sum_i Q_i = 0. \tag{12}$$

Now, the following expression holds for the charges at the minimum in E [21]:

$$Q_i = a \sum_j G_{ij} (b_j - \langle b \rangle), \tag{13}$$

where

$$G = (aI + M)^{-1}. \tag{14}$$

M denotes the Madelung matrix, and I denotes the identity matrix. This becomes

$$Q_i = a \sum_j G_{ij} b_j, \tag{15}$$

since [36]

$$\sum_j G_{ij} = 0. \tag{16}$$

Substituting Eq. (15) into Eq. (11) gives

$$E = \frac{1}{2} a \sum_i b_i^2 - \frac{1}{2} a^2 \sum_i \sum_j G_{ij} b_i b_j + E_0, \tag{17}$$

which becomes

$$E = \frac{1}{2} a b_k^2 - \frac{1}{2} a^2 G_{kk} b_k^2 - a^2 b_k \sum_{j \neq k} G_{jk} b_j + E_0 + \frac{1}{2} a \sum_{i \neq k} b_i^2 - \frac{1}{2} a^2 \sum_{i \neq k} \sum_{j \neq k} G_{ij} b_i b_j \tag{18}$$

after separating out the terms containing b_k and noting that G is a symmetric matrix [36]. We will use the above equation in a moment.

The binding energy of a core level associated with site k is

$$E_k^{\mathrm{B}} = E_k^{\mathrm{f}} - E^{\mathrm{i}}, \tag{19}$$

where E^{i} denotes the energy of the alloy's initial state, before photoemission from site k, and E_k^{f} denotes the energy of the alloy's final state, after photoemission from site k. In the complete-screening picture [42] the valence electrons in the final state are assumed to be fully relaxed so to reach their minimum-energy configuration. With this in mind, the energy of the final state is simply the energy of the initial state, but with the atomic core within k replaced by its photoionized analog. We choose site k to belong to species X, and denote the "species" corresponding to a photoionized X site as X^*. Hence, E_k^{B} is the energy change if site k, originally belonging to species X, is transformed into species X^*. Equation (18) allows us to evaluate the change in E due to such a transformation. Noting that the terms on the lower line of Eq. (18) are unaffected by the transformation (since a and b_X for all X are composition dependent, and the composition, which we defined in terms of macroscopic quantities, is unaffected by the transformation), that the transformation is such that $b_k^2 \to b_{X^*}^2 = b_X^2 + 2b_X b_{X^*X} + b_{X^*X}^2$, and also that $E_0 \to E_0 + (\mathcal{E}_{X^*} - \mathcal{E}_X)$ [see Eq. (6)], we obtain

$$\begin{aligned} E_k^{\mathrm{B}} = {} & ab_X b_{X^*X} + \frac{1}{2}ab_{X^*X}^2 - a^2 G_{kk} b_X b_{X^*X} \\ & - \frac{1}{2}a^2 G_{kk} b_{X^*X}^2 - a^2 b_{X^*X} \sum_{j\neq k} G_{jk} b_j + (\mathcal{E}_{X^*} - \mathcal{E}_X). \end{aligned} \tag{20}$$

This can be rearranged to give

$$\begin{aligned} E_k^{\mathrm{B}} = {} & \frac{1}{2}a\,(1 - aG_{kk})\, b_{X^*X}^2 + ab_X b_{X^*X} \\ & - a^2 b_{X^*X} \sum_{j} G_{jk} b_j + (\mathcal{E}_{X^*} - \mathcal{E}_X), \end{aligned} \tag{21}$$

which in turn becomes

$$\begin{aligned} E_k^{\mathrm{B}} = {} & -ab_{X^*X} Q_k + \tfrac{1}{2}a(1-\Lambda)b_{X^*X}^2 + ab_X b_{X^*X} \\ & + (\mathcal{E}_{X^*} - \mathcal{E}_X) \end{aligned} \tag{22}$$

after using Eq. (15) and noting that $\Lambda \equiv aG_{kk}$ [21]. We emphasize that Q_k in the above equation refers to the charge of site k *before* photoemission. Finally, substituting the above equation into Eq. (1) and relabeling site k as site i, we obtain the following expression for the CLS associated with site i:

$$\Delta E_i^{\mathrm{B}} = -ab_{X^*X} Q_i + \Phi_X, \tag{23}$$

where

$$\Phi_X \equiv \tfrac{1}{2}a(1-\Lambda)b_{X^*X}^2 + ab_X b_{X^*X} + (\mathcal{E}_{X^*} - \mathcal{E}_X) - E_{X\mathrm{met}}^{\mathrm{B}} \tag{24}$$

is composition dependent.

Equation (23) describes a species- and composition-dependent linear mapping between Q_i and ΔE_i^{B}. Therefore changes in the X CLS distribution associated with configuration changes—such as an increase in the interface roughening σ in a multilayer system—directly reflect changes in the X charge distribution. Furthermore the *shape* of the CLS distribution is the same as that of the charge distribution on account of the linear nature of the mapping between Q_i and ΔE_i^{B}. We will elaborate on these points later.

C. Mean and full width at half maximum of various core-level-shift distributions

Henceforth we consider the mean and FWHM of the CLS distributions for various groups of X sites. Note that the FWHM of any random variable x is related to its variance by the equation

$$\mathrm{FWHM}(x) = 2\sqrt{2\ln(2)}\sqrt{\mathrm{Var}(x)}. \tag{25}$$

We will use this fact several times below. We will also use the fact that the mean and FWHM of ΔE_i^{B} for *any group* of X sites S within a given alloy, as follows from Eq. (23), are given by

$$\langle \Delta E^{\mathrm{B}} \rangle_X^S = -ab_{X^*X} \langle Q \rangle_X^S + \Phi_X, \tag{26}$$

and

$$\Gamma_X^S = 2\sqrt{2\ln(2)}|ab_{X^*X}|\sqrt{\mathrm{Var}(Q)_X^S}, \tag{27}$$

respectively, where $\langle Q \rangle_X^S$ and $\mathrm{Var}(Q)_X^S$ denote the mean and variance, respectively, of the charge distribution for S.

1. *Random alloys*

Consider the group of all sites within a random alloy. For random alloys [21]

$$\langle Q \rangle_X = -\Lambda \sum_Y b_{YX} c_Y, \tag{28}$$

and

$$\mathrm{Var}(Q)_X = \Lambda^2 \omega\, \mathrm{Var}(b), \tag{29}$$

where $\mathrm{Var}(b)$ denotes the variance of b_i over *all sites in the system*, and ω depends only on aR_{WS} and the underlying lattice type and is tabulated in Ref. [21] for the fcc, bcc, and sc lattices. Therefore, for random alloys Eqs. (26) and (27) yield

$$\langle \Delta E^{\mathrm{B}} \rangle_X = a\Lambda \sum_Y \tilde{b}_{YX} c_Y + \Phi_X, \tag{30}$$

and

$$\Gamma_X = 2\sqrt{2\ln(2)}|a\Lambda\sqrt{\omega}| \sqrt{\sum_Y \tilde{b}_{YX}^2 c_Y - \left(\sum_Y \tilde{b}_{YX} c_Y\right)^2}, \tag{31}$$

where we have defined

$$\tilde{b}_{YX} \equiv b_{X^*X} b_{YX} \tag{32}$$

and used the fact that [21]

$$\mathrm{Var}(b) = \sum_Y b_{YX}^2 c_Y - \left(\sum_Y b_{YX} c_Y\right)^2. \tag{33}$$

For binary alloys consisting of species A and B, the above equations simplify to

$$\langle \Delta E^{\mathrm{B}} \rangle_A = a\Lambda \tilde{b}_{BA} c_B + \Phi_A, \tag{34}$$

and

$$\Gamma_A = 2\sqrt{2\ln(2)}|a\Lambda\sqrt{\omega}\tilde{b}_{BA}|\sqrt{c_B(1-c_B)}, \tag{35}$$

for $X = A$.

2. Mean for a single monolayer

Henceforth we consider the class of systems described at the beginning of this section in which the species concentrations can vary from monolayer to monolayer. Let S be the set of X sites within monolayer l. Furthermore, let $\langle \Delta E^{\mathrm{B}} \rangle_X^l$ and Γ_X^l denote the mean and FWHM, respectively, of the CLS distribution for S. A similar notation will be used later for other quantities, e.g., $\langle Q \rangle_X^l$ and $\mathrm{Var}(Q)_X^l$. We will now derive an expression for $\langle \Delta E^{\mathrm{B}} \rangle_X^l$. Consider a site i within S. From Eq. (7), Q_i can be expressed as

$$Q_i = \Lambda \sum_Y b_{YX} \sum_{\beta=1}^{\infty} g_\beta \sum_m N_{iY\beta}^m, \tag{36}$$

where $N_{iY\beta}^m$ denotes the number of Y sites in the βth nearest-neighbor shell of i which are in monolayer m. Taking the mean over all $i \in S$ gives

$$\langle Q \rangle_X^l = \Lambda \sum_Y b_{YX} \sum_{\beta=1}^{\infty} g_\beta \sum_m \langle N_{Y\beta}^m \rangle_X^l. \tag{37}$$

Now, $N_{iY\beta}^m$ over $i \in S$ describes a random variable distributed according to the multinomial distribution. Specifically, $N_{iY\beta}^m$ is the number of times outcome Y occurs in $Z_\beta^{|l-m|}$ trials, given the probability of outcome Y in a single trial is c_Y^m, where Z_β^d is the total number of sites in the βth nearest-neighbor shell of any site j which also belong to *one* monolayer which is "d monolayers away" from j—with $d = 0$ referring to the monolayer which contains site j itself. The properties of the multinomial distribution are such that $\langle N_{Y\beta}^m \rangle_X^l = Z_\beta^{|l-m|} c_Y^m$, and hence the above equation becomes

$$\langle Q \rangle_X^l = \Lambda \sum_Y b_{YX} \sum_{\beta=1}^{\infty} g_\beta \sum_m Z_\beta^{|l-m|} c_Y^m. \tag{38}$$

This can be rewritten as

$$\langle Q \rangle_X^l = \frac{1}{aR_{\mathrm{WS}}} \sum_Y b_{YX} \sum_m \alpha^{|l-m|} c_Y^m, \tag{39}$$

where we have defined

$$\alpha^d \equiv aR_{\mathrm{WS}}\Lambda \sum_{\beta=1}^{\infty} g_\beta Z_\beta^d. \tag{40}$$

Finally, substituting Eq. (39) into Eq. (26) gives

$$\langle \Delta E^{\mathrm{B}} \rangle_X^l = -\frac{1}{R_{\mathrm{WS}}} \sum_Y \tilde{b}_{YX} \sum_m \alpha^{|l-m|} c_Y^m + \Phi_X. \tag{41}$$

For species A in a binary alloy the above simplifies to

$$\langle \Delta E^{\mathrm{B}} \rangle_A^l = -\frac{\tilde{b}_{BA}}{R_{\mathrm{WS}}} \sum_m \alpha^{|l-m|} c_B^m + \Phi_B. \tag{42}$$

The quantities α^d depend on the lattice type, aR_{WS}, and the set of lattice planes which constitute the monolayers. They determine the coupling between monolayers with regards to $\langle Q \rangle_X^l$ and $\langle \Delta E^{\mathrm{B}} \rangle_X^l$. It can be shown that for the concentration profile $c_X^l = c_X$ for all l, i.e., a random alloy, the above equations become equivalent to those given earlier for random alloys. This is the case since

$$\sum_m \alpha^{|l-m|} = -aR_{\mathrm{WS}}\Lambda, \tag{43}$$

which can be shown by noting that

$$Z_\beta = \sum_m Z_\beta^m \tag{44}$$

and [21]

$$\sum_{\beta=1}^{\infty} g_\beta Z_\beta = -1. \tag{45}$$

3. FWHM for a single monolayer

We will now derive an expression for Γ_X^l. Taking the variance of Eq. (36) over $i \in S$ gives

$$\mathrm{Var}(Q)_X^l = \Lambda^2 \sum_{\beta=1}^{\infty} g_\beta^2 \sum_m \mathrm{Var}\left(\sum_Y b_{YX} N_{Y\beta}^m \right)_X^l \tag{46}$$

after noting that the random variables $N_{Y\beta}^m$ and $N_{Z\gamma}^n$, defined by considering $N_{iY\beta}^m$ and $N_{iZ\gamma}^n$ for $i \in S$, are independent if $\gamma \neq \beta$ or $n \neq m$. Expanding the variance on the right-hand side gives

$$\mathrm{Var}(Q)_X^l = \Lambda^2 \sum_{\beta=1}^{\infty} g_\beta^2 \sum_m \left[\sum_Y b_{YX}^2 \mathrm{Var}\left(N_{Y\beta}^m\right)_X^l + \sum_Y \sum_{Z \neq Y} b_{YX} b_{ZX} \mathrm{Cov}\left(N_{Y\beta}^m, N_{Z\beta}^m\right)_X^l \right], \tag{47}$$

where $\mathrm{Cov}(x,y)$ denotes the covariance of random variables x and y. Because $N_{iY\beta}^m$ over $i \in S$ form a multinomial distribution,

$$\mathrm{Var}\left(N_{Y\beta}^m\right)_X^l = Z_\beta^{|l-m|} c_Y^m \left(1 - c_Y^m\right) \tag{48}$$

and

$$\mathrm{Cov}\left(N_{Y\beta}^m, N_{Z\beta}^m\right)_X^l = -Z_\beta^{|l-m|} c_Y^m c_Z^m \quad \text{if} \quad Z \neq Y. \tag{49}$$

Substituting these equations into Eq. (47) gives

$$\mathrm{Var}(Q)_X^l = \frac{1}{(aR_{\mathrm{WS}})^2} \sum_m \beta^{|m-l|} \left[\sum_Y b_{YX}^2 c_Y^m \left(1 - c_Y^m\right) - \sum_Y \sum_{Z \neq Y} b_{YX} b_{ZX} c_Y^m c_Z^m \right], \tag{50}$$

where we have defined

$$\beta^d \equiv (aR_{\mathrm{WS}})^2\Lambda^2\sum_{\beta=1}^{\infty} g_\beta^2 Z_\beta^d. \tag{51}$$

Substituting Eq. (50) into Eq. (27) gives

$$\Gamma_X^l = 2\sqrt{2\ln(2)}\frac{1}{R_{\mathrm{WS}}}\sqrt{\sum_m \beta^{|m-l|}\left[\sum_Y \tilde{b}_{YX}^2 c_Y^m\left(1-c_Y^m\right) - \sum_Y\sum_{Z\neq Y}\tilde{b}_{YX}\tilde{b}_{ZX}c_Y^m c_Z^m\right]}. \tag{52}$$

For species A in a binary alloy the above equation simplifies significantly:

$$\Gamma_A^l = 2\sqrt{2\ln(2)}\frac{|\tilde{b}_{BA}|}{R_{\mathrm{WS}}}\sqrt{\sum_m \beta^{|m-l|}c_B^m\left(1-c_B^m\right)}. \tag{53}$$

The quantities β^d determine the coupling between monolayers with regards to $\mathrm{Var}(Q)_X^l$ and Γ_X^l. As was the case for $\langle\Delta E^{\mathrm{B}}\rangle_X^l$, if $c_X^l = c_X$ for all l then the above equations become equivalent to those given earlier for random alloys. This is the case, since

$$\sum_m \beta^{|l-m|} = (aR_{\mathrm{WS}})^2\Lambda^2\omega, \tag{54}$$

which can be shown by appealing to Eq. (44) as well as the definition of ω:

$$\omega \equiv \sum_{\beta=1}^{\infty} g_\beta^2 Z_\beta. \tag{55}$$

4. Total mean

From the quantities $\langle\Delta E^{\mathrm{B}}\rangle_X^l$ for all l, the mean CLS $\langle\Delta E^{\mathrm{B}}\rangle_X$ over *all* X sites in the system under consideration can be determined by using the following expression:

$$\langle\Delta E^{\mathrm{B}}\rangle_X = \sum_l w_X^l\langle\Delta E^{\mathrm{B}}\rangle_X^l, \tag{56}$$

where w_X^l is the *weight* to be given to monolayer l. For the "true" mean, w_X^l is given by

$$w_X^l = c_X^l \Big/ \sum_m c_X^m. \tag{57}$$

However, one is often interested in the mean of the CLS distribution observed experimentally, which may differ from the "true" value on account of the fact that the probability p^l of a photoelectron emitted from monolayer l escaping the alloy is monolayer-dependent. In this case w_X^l is given by

$$w_X^l = p^l c_X^l \Big/ \sum_m p^m c_X^m. \tag{58}$$

Equation (56) follows trivially from the following theorem: if Σ_i is a set of n_i values whose mean is μ_i, then the mean of the superset Σ formed by combining the sets Σ_i for all i is

$$\mu = \sum_i \frac{n_i}{n}\mu_i. \tag{59}$$

This result can be derived from the definitions of μ and μ_i:

$$\mu = \frac{1}{n}\sum_{\varepsilon\in\Sigma}\varepsilon = \frac{1}{n}\sum_i\sum_{\varepsilon\in\Sigma_i}\varepsilon = \sum_i\frac{n_i}{n}\left(\frac{1}{n_i}\sum_{\varepsilon\in\Sigma_i}\varepsilon\right). \tag{60}$$

5. Total full width at half maximum

From the quantities $\langle\Delta E^{\mathrm{B}}\rangle_X$, $\langle\Delta E^{\mathrm{B}}\rangle_X^l$ and Γ_X^l for all l, the FWHM in the CLS distribution over all X sites Γ_X can determined by using the following expression:

$$\Gamma_X = \sqrt{\sum_l w_X^l\left[\left(\Gamma_X^l\right)^2 + 8\ln 2\left(\langle\Delta E^{\mathrm{B}}\rangle_X^l - \langle\Delta E^{\mathrm{B}}\rangle_X\right)^2\right]}. \tag{61}$$

Equation (61) can be derived by applying Eq. (25) to the analogous equation to Eq. (59) for the variance:

$$\nu = \sum_i \frac{n_i}{n}[\nu_i + (\mu_i-\mu)^2], \tag{62}$$

where ν_i denotes the variance of Σ_i, and ν denotes the variance of Σ. The above equation can itself be derived somewhat similarly to Eq. (59):

$$\begin{aligned}\nu &= \frac{1}{n}\sum_{\varepsilon\in\Sigma}(\varepsilon-\mu)^2 = \sum_i\frac{n_i}{n}\frac{1}{n_i}\sum_{\varepsilon\in\Sigma_i}(\varepsilon-\mu)^2\\ &= \sum_i\frac{n_i}{n}\frac{1}{n_i}\sum_{\varepsilon\in\Sigma_i}[(\varepsilon-\mu_i)+(\mu_i-\mu)]^2\\ &= \sum_i\frac{n_i}{n}\left[\frac{1}{n_i}\sum_{\varepsilon\in\Sigma_i}(\varepsilon-\mu_i)^2 + (\mu_i-\mu)^2\right.\\ &\quad\left. + 2\frac{1}{n_i}(\mu_i-\mu)\sum_{\varepsilon\in\Sigma_i}(\varepsilon-\mu_i)\right],\end{aligned} \tag{63}$$

which becomes Eq. (62) after noting that the final term in the last equality vanishes.

III. COMPUTATIONAL DETAILS

In the next section we apply the expressions of Sec. II C to various multilayer systems. All systems we consider have an fcc underlying lattice, and the monolayers are the 001 planes. However, to apply these expressions we first had to determine the monolayer coupling parameters α^d and β^d, which are defined in Eqs. (40) and (51). In Ref. [21], Λ and g_β are tabulated as a function of aR_{WS} for the fcc, bcc, and sc lattices. By using this information, and after determining the quantities

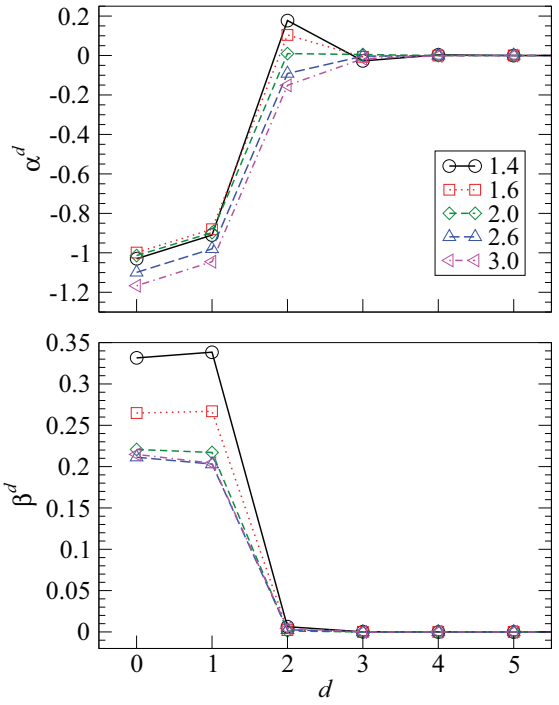

FIG. 2. (Color online) The monolayer coupling parameters α^d and β^d for the 001 planes in the fcc lattice for various values of aR_{WS}. The top panel shows α^d vs d, while the bottom panel shows β^d vs d. The aR_{WS} to which each curve corresponds can be deduced from the key in the top panel.

Z^d_β—which depend on the underlying geometry—one can tabulate α^d and β^d as a function of aR_{WS} for any fcc, bcc, or sc system. For other lattice types, Λ and g_β must be determined as a function of aR_{WS} beforehand. A procedure to do this is described in Ref. [21]. We determined α^d and β^d for the 001 planes of the fcc lattice at selected aR_{WS}. The results are shown in Fig. 2. We considered $aR_{\mathrm{WS}} = 1.4$, 1.6, 2.0, 2.6, and 3.0, which reflects the range of aR_{WS} found in the literature [17,37–40,43,44]. Note that the coupling between monolayers rapidly tends to zero with d.

In addition to the aforementioned "analytical" results, we also performed supercell calculations for each of the systems we considered. In our supercells, each monolayer contained 200 sites, with the species of sites in each monolayer l assigned randomly such that the desired species concentrations c^l_X were obtained as closely as possible. ΔE^{B}_i was determined for each site by using Eqs. (23) and (7). These ΔE^{B}_i where then used to determine $\langle \Delta E^{\mathrm{B}} \rangle^l_X$, Γ^l_X, $\langle \Delta E^{\mathrm{B}} \rangle_X$, and Γ_X in the conventional manner, which allowed us to cross-check our analytical results. For all systems the analytical and supercell results were in excellent agreement, though we choose not to present the supercell means and FWHMs for the sake of brevity and clarity of presentation. In addition to cross-checking, the supercell values of ΔE^{B}_i were used to simulate core-level spectra for some systems. In this regard we used the following equation:

$$I(\Delta E^{\mathrm{B}}) = \sum_{i \in X} L\left(\Delta E^{\mathrm{B}} - \Delta E^{\mathrm{B}}_i; \Gamma_{\mathrm{life}}\right), \tag{64}$$

where $I(\Delta E^{\mathrm{B}})$ denotes the intensity of the X spectrum at CLS ΔE^{B}, $L(\Delta E^{\mathrm{B}}; \Gamma)$ is a Lorentzian function with FWHM Γ, and Γ_{life} is the lifetime broadening of the core levels under consideration. The above equation does not take into account many features which are present in "real" spectra such as surface core-level shifts, experimental broadening, Doniac–Sunjic asymmetry, and inelastic scattering. However, since our simulated spectra are primarily for illustrative purposes, ignoring these complications is justified. Our supercell calculations served one further purpose. Later, for binary systems, we present histograms of the frequency of A sites exhibiting each possible number of B nearest neighbors and, for ternary systems, the frequency of A sites exhibiting each possible combination of B and C nearest neighbors. We used our supercells to generate these histograms: for each supercell we counted the number of A sites with each possible composition of nearest-neighbor shell.

IV. RESULTS

A. Isolated embedded thin film: $B/A_T/B$

We first present results for systems consisting of a thin film of species A and thickness T monolayers embedded in a B substrate, i.e., $B/A_T/B$. We examined such systems with various T and σ, where recall that σ denotes the degree of interface roughening. Following Refs. [17,34], interface roughening was modeled by convoluting the "unroughened" concentration profile with a discrete Gaussian function [34], where σ denotes the standard deviation of the function. To elaborate, the concentration profile corresponding to σ was calculated using the following equation:

$$c^l_X(\sigma) = \sum_m \gamma^{l-m}(\sigma) c^l_X(0) \tag{65}$$

for all X, where

$$\gamma^d(\sigma) = \frac{\exp[-(d/\sigma)^2/2]}{\sum_{d'=-\infty}^{\infty} \exp[-(d'/\sigma)^2/2]} \tag{66}$$

is the discrete analog of a Gaussian function with standard deviation σ, and $c^l_X(0)$ denotes the unroughened concentration profile.

1. General results

The quantities $\langle \Delta E^{\mathrm{B}} \rangle^l_A$, $\langle \Delta E^{\mathrm{B}} \rangle_A$, Γ^l_A, and Γ_A for various $B/A_T/B$ systems are presented in Figs. 3 and 4. In calculating these values, we used the set of aR_{WS} described in the previous section. Furthermore, we set $R_{\mathrm{WS}} = 1$, $\tilde{b}_{BA} \equiv b_{A^*A} b_{BA} = -1$, and $\Phi_A = 0$. Results (in eV) obtained by using these parameters can be generalized to any choice of R_{WS} (in bohrs), b_{A^*A}, b_{BA} (both in units of e), and Φ_A (in eV) at the corresponding value of aR_{WS} by multiplying all means and FWHMs by $-b_{A^*A} b_{BA}/R_{\mathrm{WS}}$, and additionally adding Φ_A to all mean CLSs. We will use this fact in a moment.

Some interesting results are immediately apparent from Figs. 3 and 4. First, as can be seen from both figures, the model results only depend weakly on aR_{WS}. This is convenient because the "true" value of aR_{WS} for a given system is unclear;

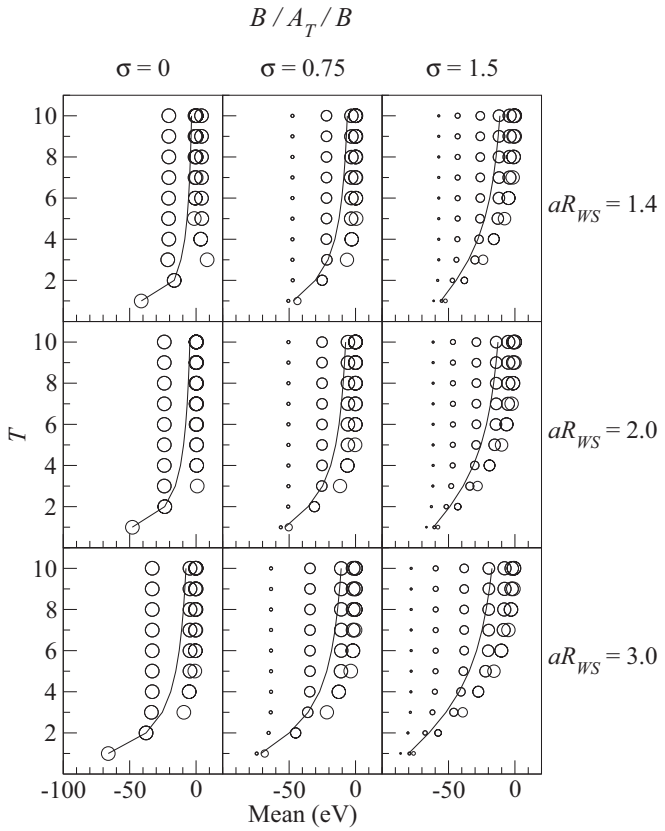

FIG. 3. Mean CLSs for $B/A_T/B$ systems calculated by using the model. Each column pertains to a different value of σ, which is indicated above the column; each row pertains to a different value of aR_{WS}, which is indicated to the right of the row. Each circle represents $\langle \Delta E^{\mathrm{B}} \rangle_A^l$ for a particular monolayer l; the size of the symbol is proportional to c_A^l. Only results pertaining to monolayers with $c_A^l > 0.05$ are shown. The solid lines connect $\langle \Delta E^{\mathrm{B}} \rangle_A$ for each value of T.

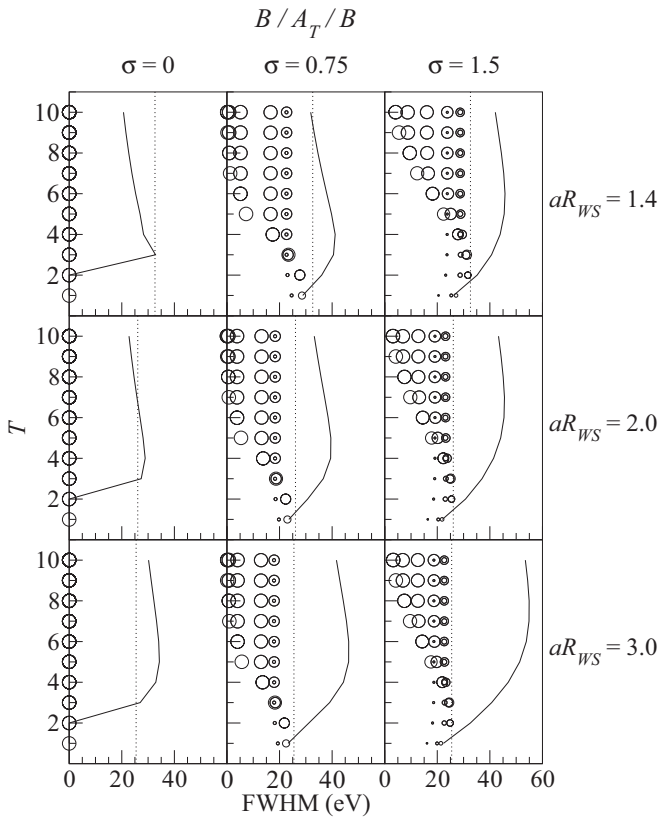

FIG. 4. FWHM CLSs for $B/A_T/B$ systems calculated by using the model. The details of the figure are the same as for Fig. (3), except that circles represent Γ_A^l, and solid lines connect Γ_A for each value of T. Furthermore, the dotted line in each panel corresponds to the upper bound on the FWHM of a random alloy at the corresponding value of aR_{WS}.

values of aR_{WS} are very sensitive to the *ab initio* method used to obtain them. The same is true for the quantities b_{YX}, and presumably also for the quantities b_{X^*X} and Φ_X. This is illustrated in Table I, where aR_{WS} and b_{CuZn} for the bcc random alloy $\mathrm{Cu}_{0.5}\mathrm{Zn}_{0.5}$ obtained by using different *ab initio* methods are compared. In calculating each aR_{WS} in the table we took a to be the mean of the *ab initio* Q-V–relation gradients a_{Cu} and a_{Zn} for Cu and Zn. Furthermore, we calculated b_{CuZn} from the Q-V–relation intercepts via $b_{\mathrm{CuZn}} = (k_{\mathrm{Cu}} - k_{\mathrm{Zn}})/a$ [see Eq. (5)].

Our second observation relates to Fig. 4. One might expect that, at a given composition and parametrization of the model (i.e., choice of the quantities aR_{WS}, b_{A^*A}, b_{BA}, and Φ_A), the A FWHM would be maximized at the random alloy configuration. This configuration corresponds to the largest configurational entropy, and therefore might be expected to exhibit the largest range of environments and hence also the largest FWHM. Moreover, since, as can be seen from Eq. (35), $\sqrt{c_B(1-c_B)}$ is maximized when $c_A = c_B = 0.5$, one might therefore also expect that the corresponding FWHM, which is an upper bound for the FWHM of a random alloy, is also an upper bound for *all* alloys. However, our results reveal that this is *not* the case. In each panel of Fig. 4, the random alloy upper bound corresponding to the same model parametrization as we used for our $B/A_T/B$ systems is indicated by a dotted line. Note that, for some systems, Γ_A is significantly larger than the random alloy upper bound. It is even possible for the upper bound to be exceeded in unroughened ultrathin films—as is evident from the left-most column in Fig. 4. Therefore inhomogeneous concentration profiles can yield larger disorder broadenings than is possible in random alloys—a fact which we explain later. A similar observation has been made in our earlier study [20] by using the linear charge model [45]: surface segregation was shown

TABLE I. aR_{WS} and b_{CuZn} for $\mathrm{Cu}_{0.5}\mathrm{Zn}_{0.5}$ obtained using various *ab initio* calculations. The abbreviation "LSMS" refers to the locally self-consistent Green's function method; and "LAPW" refers to the linearized augmented plane-wave method. See Refs. [37–39] and references therein for details regarding these calculations.

Method	aR_{WS}	b_{CuZn}
LSMS [38,39,43]	2.5	0.16
GCPA [37]	1.6	0.12
LAPW [37]	3.5	0.16

to result in a significantly larger disorder broadening relative to the unsegregated random alloy. However in that study surface effects are implicit in the simulated spectra and hence cannot be discounted as a contributing factor to the very large broadening. By contrast, here we have shown that a very large broadening can occur in the absence of surface effects. In the aforementioned study we suggested that segregation could explain the anomalously large disorder broadening observed experimentally by Medicherla *et al.* [46]. Our results here provide further evidence for this hypothesis.

In contrast to Γ_A, the monolayer FWHMs Γ_A^l seem to be constrained to be below the random alloy upper bound. This can be understood by noting that the A sites in monolayer l experience a local environment which closely resembles a random alloy, and hence Γ_A^l (to a good approximation) cannot exceed the upper bound. Considering only nearest neighbors, each A site in monolayer l has Z_1^0 nearest neighbors in monolayer l, Z_1^1 in monolayer $l-1$, and Z_1^1 in monolayer $l+1$. Since *within each monolayer* we have randomly assigned the species of sites in the required concentrations, it follows that the environment of an A site in monolayer l is approximately that of a random alloy with concentration

$$c_{A,\mathrm{eff}}^l \approx Z_1^0 c_A^l + Z_1^1 c_A^{l-1} + Z_1^1 c_A^{l+1}. \tag{67}$$

2. *Comparison with ab initio results*

The $B/A_T/B$ systems we considered were deliberately chosen to be identical to the fcc systems considered in Ref. [17], in which Olovsson *et al.* calculated $\langle \Delta E^{\mathrm{B}} \rangle_{\mathrm{Cu}}^l$ for Ni/Cu$_T$/Ni and Co/Cu$_T$/Co. The $\langle \Delta E^{\mathrm{B}} \rangle_{\mathrm{Cu}}^l$ and $\langle \Delta E^{\mathrm{B}} \rangle_{\mathrm{Cu}}^l$ determined by Olovsson *et al.* are shown in Fig. 5. Comparing this figure with Fig. 3 we see that the model is in excellent qualitative agreement with those of Olovsson *et al.* for the Ni/Cu$_T$/Ni systems. The agreement is especially good at higher values of aR_{WS}. For the Co/Cu$_T$/Co systems, the agreement is reasonable. However, it should be borne in mind that the dispersion of CLSs in Co/Cu$_T$/Co is very small, and hence any uncertainties implicit in the *ab initio* method used by Olovsson *et al.* will be larger relative to the size of the dispersion: Olovsson *et al.* quote CLSs to a precision of 10 meV, which is significant on the scale of the Co/Cu$_T$/Co dispersion, but not for the Ni/Cu$_T$/Ni dispersion.

The R_{WS} used by Olovsson *et al.* in their calculations was 2.6 bohrs for both Ni/Cu$_T$/Ni and Co/Cu$_T$/Co. With this in mind, and recalling the procedure described above for generalizing our model results to different free parameters, we found that $aR_{\mathrm{WS}} \approx 2.6$, $\Phi_{\mathrm{Cu}} \approx 0.15$ eV, and $b_{\mathrm{Cu^*Cu}} b_{\mathrm{NiCu}} \approx -0.015e^2$ gave excellent agreement with Olovsson *et al.* for Ni/Cu$_T$/Ni. For Co/Cu$_T$/Co we found acceptable agreement when $aR_{\mathrm{WS}} \approx 2.6$, $b_{\mathrm{Cu^*Cu}} b_{\mathrm{CoCu}} \approx -0.01e^2$, and $\Phi_{\mathrm{Cu}} \approx 0.2$ eV. These values are similar to analogous quantities obtained from *ab initio* calculations for other alloys [17,37–40,43,44]. However, as mentioned earlier, the values of these quantities are sensitive to the *ab initio* method used to obtain them. Hence an interesting prospect is to use the model to determine their values experimentally.

Olovsson *et al.* used the $\langle \Delta E^{\mathrm{B}} \rangle_{\mathrm{Cu}}^l$ from their calculations to simulate core-level XPS spectra. However, since their calculations did not provide values for Γ_{Cu}^l, it was necessary for Olovsson *et al.* to make some assumptions regarding

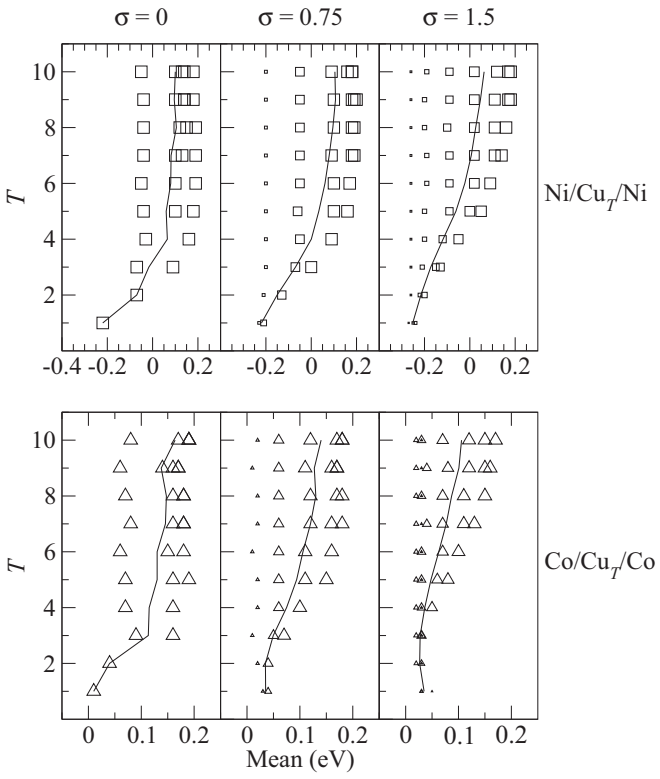

FIG. 5. Mean CLSs for Ni/Cu$_T$/Ni and Co/Cu$_T$/Co systems calculated by Olovsson *et al.* (Ref. [17].). The significance of each column, and the symbols and lines, is the same as in Fig. 3. The top row of graphs corresponds to Ni/Cu$_T$/Ni, while the bottom row corresponds to Co/Cu$_T$/Co.

these quantities. They assumed that Γ_{Cu}^l was the same for all l. Figure 4 reveals that, in fact, the quantities Γ_{Cu}^l vary widely within any one system. Hence the assumption made by Olovsson *et al.* is incorrect. However, it is unclear whether the breakdown of this assumption is important from a practical point of view. While accurate knowledge of the quantities Γ_X^l—as well as perhaps higher moments of the X CLS distribution for each monolayer—is necessary to reproduce the fine details of the total X CLS distribution for the system under consideration, in practice these fine details are "smeared out" in the experimental spectrum due to complications such as lifetime and experimental broadening. Therefore getting some of the fine details wrong in the spectrum before accounting for the aforementioned complications may be inconsequential with regards to accurately reproducing experimental spectra.

It should be noted that Olovsson *et al.* considered a further system in their study in addition to Ni/Cu$_T$/Ni and Co/Cu$_T$/Co: Fe/Cu$_T$/Fe. We do not perform a thorough comparison between our model calculations and those of Olovsson *et al.* for Fe/Cu$_T$/Fe because the underlying lattice for Fe/Cu$_T$/Fe is bcc, while our model calculations are for a fcc underlying lattice. At $\sigma = 0.75$ and $\sigma = 1.5$, the qualitative nature of the *ab initio* Fe/Cu$_T$/Fe results is similar to that for Ni/Cu$_T$/Ni and Co/Cu$_T$/Co. In these cases we therefore expect that the model will perform well for Fe/Cu$_T$/Fe. However, as pointed out by Olovsson *et al.*, a well-known interface state exists in ordered, but not in disordered, Fe/Cu$_T$/Fe systems, which

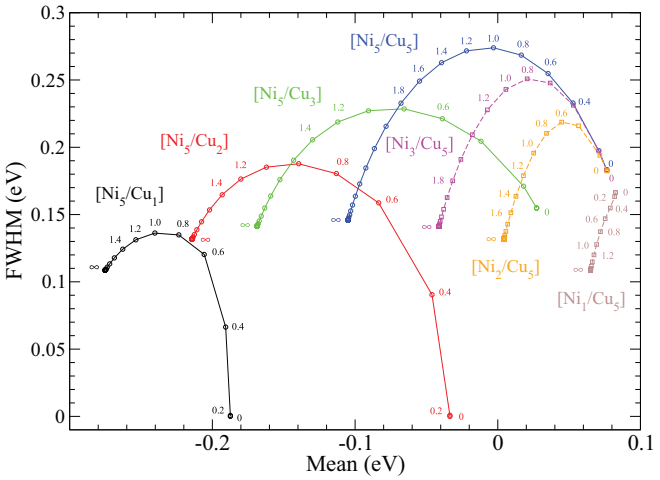

FIG. 6. (Color online) Mean and FWHM of the Cu CLS distribution in various NiCu systems as a function of σ, determined by using the model. Each color pertains to a different system; each system is labeled. Symbols indicate the (mean, FWHM) evaluated at σ from 0 to ∞ at intervals of σ of 0.2. Some of the symbols are annotated with their value of σ. Curves connect the symbols and trace the (mean, FWHM) from $\sigma = 0$ to $\sigma = \infty$ for each system.

causes "anomalous" results for $\sigma = 0$. It would be interesting to see whether model calculations utilizing a bcc lattice can reproduce this.

B. Periodic NiCu multilayers: [Ni$_T$/Cu$_U$]

In the previous section we considered an isolated thin film embedded in an infinite substrate. This was done primarily to allow comparison with analogous *ab initio* results. However, experimental studies have focused on *periodic* multilayer systems. We now consider such systems; specifically, those comprised of Ni and Cu in which the repeating unit consists of T monolayers of Ni adjacent to U monolayers of Cu, i.e., [Ni$_T$/Cu$_U$]. We considered various T, U, and σ. As above, we used Eq. (65) to obtain the concentration profile for a given σ. With regards to the parametrization of the model, we used the "best-fit parametrization" described above for the Ni/Cu$_T$/Ni systems, i.e., $aR_{\mathrm{WS}} = 2.6$, $\Phi_{\mathrm{Cu}} = 0.15$ eV, and $b_{\mathrm{Cu^*Cu}} b_{\mathrm{NiCu}} = -0.015e^2$.

The $\langle \Delta E^{\mathrm{B}} \rangle_{\mathrm{Cu}}$ and Γ_{Cu} for various [Ni$_T$/Cu$_U$] systems as a function of σ are presented in Fig. 6; we show the "trajectory" of the pair $(\langle \Delta E^{\mathrm{B}} \rangle_{\mathrm{Cu}}, \Gamma_{\mathrm{Cu}})$ as σ is varied from 0 to ∞. Note that at $\sigma = \infty$ intermixing between the Ni and Cu regions is absolute, and [Ni$_T$/Cu$_U$] becomes a random alloy with $c_{\mathrm{Cu}} = U/(T+U)$. As is evident from Fig. 6, as σ increases, $\langle \Delta E^{\mathrm{B}} \rangle_{\mathrm{Cu}}$ becomes more negative, and Γ_{Cu} increases initially, before decreasing and finally settling on the random alloy value. The exception is [Ni$_1$/Cu$_5$], for which Γ_{Cu} monotonically decreases with σ, i.e., the system exhibits a "disorder narrowing." We will now explain these trends.

1. Rationalization of spectral changes

A pleasing feature of the model is that it provides a simple means of rationalizing changes in CLS spectra due to configurational changes. Consider Eq. (7). An insightful approximation is to ignore the dependence of Q_i on the environment of site i beyond its nearest-neighbor shell, in which case for Cu in NiCu systems the number of Ni nearest neighbors $N_{i\mathrm{Ni1}}$ of site i wholly determines Q_i [50]. Specifically, Q_i is linear in $N_{i\mathrm{Ni1}}$:

$$Q_i \approx \Lambda g_1 b_{\mathrm{NiCu}} N_{i\mathrm{Ni1}}. \tag{68}$$

The same then applies to ΔE_i^{B} [from Eq. (23)]:

$$\Delta E_i^{\mathrm{B}} \approx -a\Lambda g_1 b_{\mathrm{Cu^*Cu}} b_{\mathrm{NiCu}} N_{i\mathrm{Ni1}} + \Phi_{\mathrm{Cu}}. \tag{69}$$

By using the above expression, the Cu spectrum can be decomposed into, or constructed from, components associated with Cu atoms with each value of $N_{i\mathrm{Ni1}}$, which allows us to equate changes in the Cu spectrum to changes in the system's "$N_{i\mathrm{Ni1}}$ histogram" for Cu.

This is done in Fig. 1(b) for [Ni$_5$/Cu$_5$], where we have used $\Gamma_{\mathrm{life}} = 0.3$ eV in the simulated spectra. At $\sigma = 0$ Cu sites exhibit only two possible environments, $N_{i\mathrm{Ni1}} = 0$ or 4, with the former corresponding to the three "central" monolayers of the five-monolayer Cu stack and the latter corresponding to the two "edge" monolayers. On the whole, Cu sites exhibit higher values of $N_{i\mathrm{Ni1}}$ as Cu diffuses into the Ni region, leading to a shift in the spectrum to low binding energies as σ increases. The width of the spectrum increases as the $N_{i\mathrm{Ni1}}$ histogram becomes "flat" near $\sigma = 1.5$, and then narrows again as $\sigma \to \infty$ and the histogram tends to that corresponding to the random alloy Ni$_{0.5}$Cu$_{0.5}$. Note that, as we found earlier to be the case for the $B/A_T/B$ systems, the disorder broadening is not maximized at the random alloy configuration. An explanation for this is as follows: The $N_{i\mathrm{Ni1}}$ histograms for random alloys—substitutionally disordered systems with homogeneous concentration profiles—are binomial distributions. For inhomogeneous concentration profiles, such as those for [Ni$_5$/Cu$_5$] at $\sigma \neq \infty$, the histograms are not constrained to be binomial distributions—they are free to be "flatter." Therefore, systems with inhomogeneous concentration profiles can exhibit significantly larger disorder broadenings than random alloys—as is borne out in Figs. 1(b), 4, and 6.

As another example, consider [Ni$_1$/Cu$_5$], which we earlier pointed out exhibits a disorder narrowing. Figure 7 is analogous to Fig. 1, but for [Ni$_1$/Cu$_5$]. Again, we used $\Gamma_{\mathrm{life}} = 0.3$ eV in the simulated spectrum. At $\sigma = 0$ the Cu sites in the two edge monolayers of a five-monolayer Cu stack have $N_{i\mathrm{Ni1}} = 4$, while the Cu sites in the three central monolayers have $N_{i\mathrm{Ni1}} = 0$. This is in fact exactly the same situation as for [Ni$_5$/Cu$_5$]. As σ is increased, the Cu sites begin to exhibit other values of $N_{i\mathrm{Ni1}}$; some Cu sites begin to "occupy" the $N_{i\mathrm{Ni1}} = 1-3$ "states" which were unoccupied at $\sigma = 0$. The same also occurs in [Ni$_5$/Cu$_5$]. However, by comparing Figs. 1 and 7 it can be seen that there is a significant occupation of the $N_{i\mathrm{Ni1}} > 4$ states in [Ni$_5$/Cu$_5$] which does not occur in [Ni$_1$/Cu$_5$] on account of the lack of Ni. Hence, in [Ni$_1$/Cu$_5$], loosely speaking, the Cu sites spill from their $N_{i\mathrm{Ni1}} = 0$ and $N_{i\mathrm{Ni1}} = 4$ states into only the $N_{i\mathrm{Ni1}} = 1$–3 states as σ is increased, which results in a narrowing of the spectrum in this system.

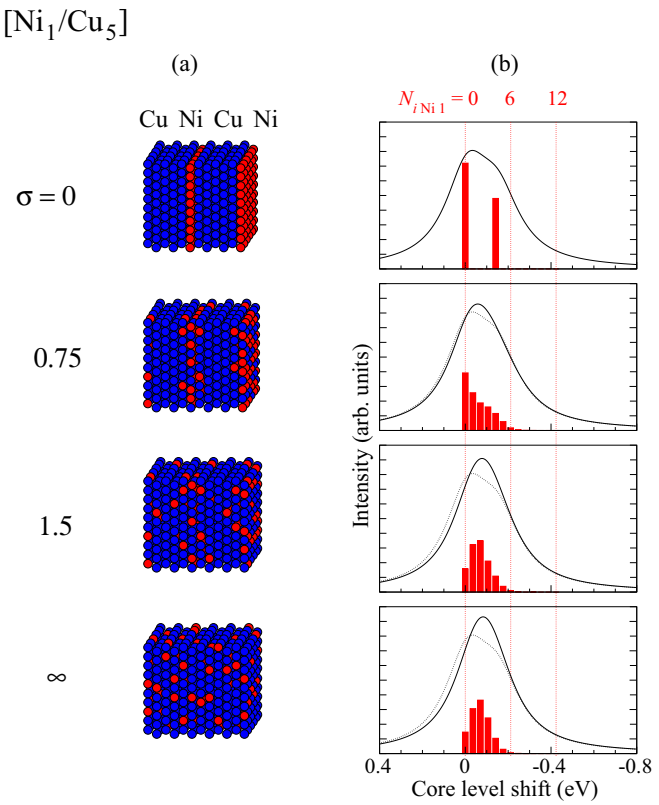

FIG. 7. (Color online) The details of this figure are the same as for Fig. 1, except that this figure pertains to the alloy system $[Ni_1/Cu_5]$.

2. *Comparison with experimental results*

Experimental Cu spectra for $[Ni_5/Cu_5]$ and $[Ni_5/Cu_2]$ at various temperatures were obtained in Refs. [7,8]. However, the spectra were found to depend strongly on the material used to cap the sample, and also on the photon energy used [8]. This is due to the finite escape depth of the photoelectrons, which leads to Cu sites near the surface being "over represented" in the Cu spectra. Our model results do not account for such surface effects; they pertain to the deep bulk. Hence, a quantitative comparison between our model results and most of the experimental spectra is meaningless. The possible exception is the spectra for $[Ni_5/Cu_5]$ in Ref. [8] taken by using a photon energy of 6030 eV—which corresponds to a relatively low surface sensitivity. These spectra reveal a shift of ≈ -0.2 eV in $[Ni_5/Cu_5]$ upon heating over the temperature range corresponding to the transition from $\sigma = 0$ to $\sigma = \infty$. This is in excellent agreement with our results: as can be seen from Fig. 6, from $\sigma = 0$ to $\sigma = \infty$ the model predicts a shift in the Cu CLS of ≈ -0.2 eV for $[Ni_5/Cu_5]$. In the future it would be interesting to perform model calculations which take into account surface effects, and which therefore can be compared directly with the results of Refs. [7,8].

C. Ternary systems

Finally, we consider ternary multilayer systems—consisting of three species A, B, and C. Recall that the X CLS distribution reflects the X charge distribution [Eq. (23)], which itself is determined by charge transfer between X and non-X sites [Eq. (7)]. In binary systems, Eq. (7) gives

$$\begin{aligned} Q_i &= \Lambda b_{BA} \sum_{\beta=1}^{\infty} g_\beta N_{iB\beta} \quad \text{if} \quad i \in A, \\ Q_i &= -\Lambda b_{BA} \sum_{\beta=1}^{\infty} g_\beta N_{iA\beta} \quad \text{if} \quad i \in B, \end{aligned} \tag{70}$$

where we have used the fact that $b_{YX} = -b_{XY}$. Without loss of generality, let $b_{BA} > 0$, which corresponds to choosing species A to be the most electronegative of A and B. From the above equations it can be seen that the electropositivity difference b_{BA} between species B and A acts only as a scale factor for the A and B charge distributions; altering b_{BA} has no effect on the *qualitative* nature of the A and B charge distributions. Ternary systems are more complicated. The analogous equation to the above for species A in a ternary system is

$$Q_i = \Lambda \left[b_{BA} \sum_{\beta=1}^{\infty} g_\beta N_{iB\beta} + b_{CA} \sum_{\beta=1}^{\infty} g_\beta N_{iC\beta} \right]. \tag{71}$$

Note that altering b_{BA} affects the charge transfer between site i and local B sites, while leaving the transfer with local C sites unaffected; and conversely if b_{CA} is altered. Hence altering b_{CA} or b_{BA} nontrivially alters the A charge distribution. In this sense ternary systems are extremely rich. An exhaustive survey of what can be expected from such systems is beyond the scope of this work. We instead limit ourselves to two ternary systems which we have found to exhibit somewhat counterintuitive behaviors. Furthermore, we limit our discussion to the qualitative aspects of these systems, with a focus on understanding these behaviors. For both systems species A is the focus of our attention.

1. *Periodic ternary multilayer:* $[B_5/A_5/C_5]$

The first ternary system we consider is $[B_5/A_5/C_5]$. Again, we use Eq. (65) to model the interface roughening; Fig. 8(a) gives a schematic illustration of the system at the σ we considered. For our calculations we set the electropositivities of each species to be $b_B = -1$, $b_A = 0$, and $b_C = 1$: the electropositivity of species A is exactly halfway between those of species B and C, with species B being the most electronegative and species C being the most electropositive. With regards to the other model parameters we set $\Phi_A = 0$, $aR_{\rm WS} = 2.0$, $R_{\rm WS} = 1$, $b_{A^*A} = 1$, and $\Gamma_{\rm life} = 35$. Figure 8(c) shows the simulated A spectra at each σ. As is evident from the figure, the mean of the A CLS distribution is independent of σ. Hence here one cannot use the mean to characterize σ in this system—one must use the FWHM. This stems from the choice of species electropositivities. Charge transfer from B to A and C to A is always equal and opposite on account of the electropositivity of A being exactly between that of B and C. This, in conjunction with the symmetry of the system, always yields a global mean A charge of 0 regardless of σ and, hence, from Eq. (23), a σ-independent mean CLS. Another interesting feature of this system is that the $\sigma = 0$ and $\sigma = \infty$ spectra are ostensibly indistinguishable. Hence, unambiguously determining σ in this system from the A spectrum alone is difficult.

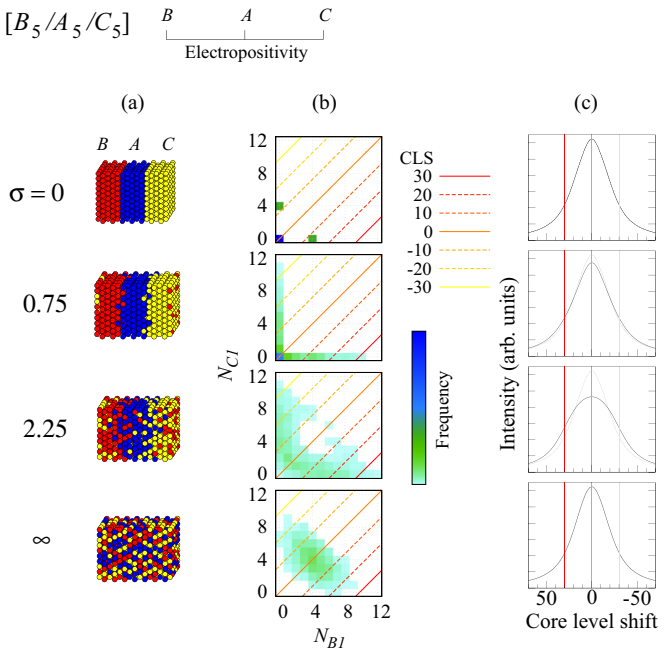

FIG. 8. (Color online) (a) Schematic illustration of $[B_5/A_5/C_5]$ at various σ, (b) the corresponding (N_{B1},N_{C1}) histograms and environment vs CLS maps for species A and (c) model spectra. In panel (b), the green-blue squares represents the frequency of A sites with the environment (N_{B1},N_{C1}), and yellow-red curves are contours of constant CLS determined according to Eq. (72). In panel (c) the dotted curves are spectra for $\sigma = 0$, and the location of some of the CLS contours in panel (b) is also shown.

The method described earlier for rationalizing spectral changes in binary systems can be extended to ternary systems. The analogous equation to Eq. (69) for species A in a ternary system is

$$\Delta E_i^{\mathrm{B}} \approx -a\Lambda g_1 b_{A^*A}[b_{BA}N_{iB1} + b_{CA}N_{iC1}] + \Phi_A. \qquad (72)$$

Note that here ΔE_i^{B} depends on the environment of i through the pair (N_{iB1},N_{iC1}); there is a mapping from (N_{iB1},N_{iC1}) to ΔE_i^{B}. Hence the A spectrum reflects the "(N_{iB1},N_{iC1}) histogram" of species A. This is illustrated in Figs. 8(b)–8(c). Figure 8(b) illustrates the frequency of A sites with each (N_{iB1},N_{iC1}) [i.e., the (N_{iB1},N_{iC1}) histogram for species A], and the CLS for each (N_{iB1},N_{iC1}) are drawn as contours of constant CLS in "(N_{iB1},N_{iC1}) space". If an environment (N_{iB1},N_{iC1}) is exhibited by a high frequency of sites, then there is a spike in the CLS spectrum at the corresponding CLS. This allows rationalization of the evolution of the A spectrum with σ. At $\sigma = 0$ there are only three possible environments for A sites: $(N_{iB1},N_{iC1}) = (4,0)$, which corresponds to a site adjacent to the B region; $(0,4)$, which corresponds to a site adjacent to the C region; and $(0,0)$, which corresponds to a site in the center of the A region—surrounded by A sites. At $\sigma = 0.75$ there is a small amount of intermixing at the interfaces. This leads to A sites near the B region exhibiting environments $(1,0)$, $(2,0)$, $(3,0)$, etc.; and A sites near the C region exhibiting environments $(0,1)$, $(0,2)$, $(0,3)$, etc. Note that at this point no A sites have both B *and* C nearest neighbors, and hence the frequency of any environment (N_{iB1},N_{iC1}) is only nonzero if $(N_{iB1},N_{iC1}) = (x,0)$ or $(0,x)$ for any x. With regards to the spectrum, the "spreading out" of the histogram along the left and bottom edges means that environments are exhibited which correspond to more extreme CLSs, i.e., $\Delta E_i^{\mathrm{B}} \approx 30$ and ≈ -30. Hence the spectrum broadens from $\sigma = 0$ to 0.75. At $\sigma = 2.25$ the interface roughening is large enough that there are A sites with both B and C neighbors, and hence there is a nonzero frequency for environments away from the left and lower edges of the (N_{iB1},N_{iC1}) histogram. At $\sigma = \infty$ we have a ternary random alloy, and the (N_{iB1},N_{iC1}) histogram corresponds to that of a trinomial distribution.

2. *Intermixing near an immiscible thin film: $A_5/B_5/C$*

The final system we consider is $A_5/B_5/C$, with A constrained to be immiscible in B and C, and the electropositivities set to $b_A = 0$, $b_C = 0.1$, and $b_B = 1$. The electropositivities correspond to the following situation: species A is the most electronegative, species B is the most electropositive, and species C has an intermediate electropositivity very close to that of species A. This system is interesting because, like $[Ni_1/Cu_5]$ discussed earlier, it exhibits a disorder narrowing. Constraining A to be immiscible in B and C renders Eq. (65) unsuitable. We therefore instead modeled the interface roughening for this system using the equation

$$c_X^l(\sigma) = \sum_{m=1}^{\infty}[\gamma^{l-m}(\sigma) - \gamma^{l+m}(\sigma)]c_X^l(\sigma = 0) \qquad (73)$$

for $X = B,C$, where we have used the convention that the interface between species A and B at $\sigma = 0$ is located between monolayers 0 and 1. The resulting concentration profiles are illustrated in Fig. 9(a). Similarly to Fig. 8, Figs. 9(b) and 9(c) show the (N_{iB1},N_{iC1}) histogram and simulated spectra for

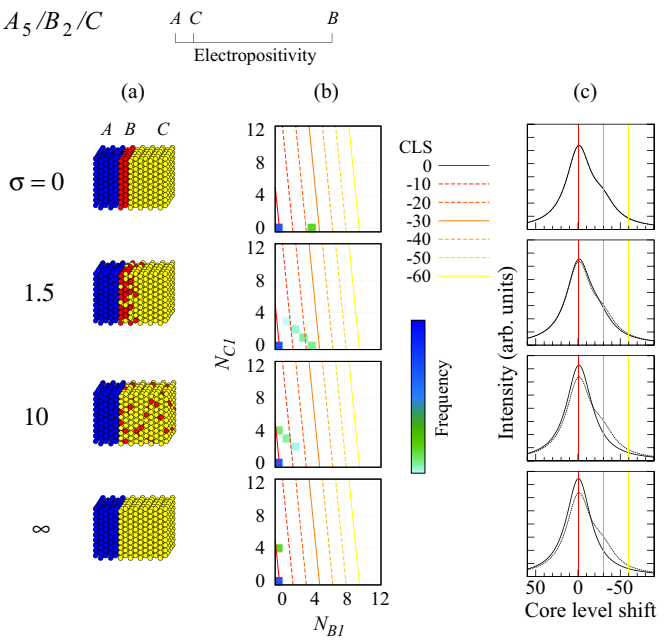

FIG. 9. (Color online) The details of this figure are the same as for Fig. 8, except that this figure pertains to the alloy system $A_5/B_2/C$.

species A at each of the considered σ. For this system we used the same Φ_A, $aR_{\rm WS}$, $R_{\rm WS}$, b_{A^*A}, and $\Gamma_{\rm life}$ as for $[B_5/A_5/C_5]$.

Earlier we saw that $[{\rm Ni}_1/{\rm Cu}_5]$ exhibits a disorder narrowing. In general, given that the A spectrum of a system reflects the A charge distribution—as follows from Eq. (23)—a disorder narrowing for A occurs when the introduction of substitutional disorder "quenches" the width of the A charge distribution. This occurs here. Species B and A transfer a certain amount of charge, which results in an A charge distribution with a certain width at $\sigma = 0$. As σ is increased, more C sites come within the charge-transfer range of the A region. Given the tiny electropositivity difference between species A and C, there is almost no charge transfer between A and C sites. Hence the influx of C sites to the A interface acts to reduce the charges of the edge A sites, bringing them closer to that of the "nonedge" A sites. This corresponds to a reduction in the width of the A charge distribution, and hence also the core-level spectrum. Alternatively, one can explain the disorder narrowing in terms of the evolution of the (N_{iB1}, N_{iC1}) histogram for species A [Fig. 9(b)]. At $\sigma = 0$ the environment of the A sites on the edge monolayer is $(N_{iB1}, N_{iC1}) = (4,0)$, which steadily transitions to $(N_{iB1}, N_{iC1}) = (0,4)$ as $\sigma \to \infty$. The latter environment has a CLS closer to that of the nonedge A sites, i.e., $(N_{iB1}, N_{iC1}) = (0,0)$, and hence the spectrum narrows as σ is increased.

V. SUMMARY AND DISCUSSION

Above we presented a model for core-level shifts in alloys and used it to add insight into the relationship between atomic environment, charge transfer, and disorder broadening in complex systems. Our key result is that the mapping between the distribution of atomic environments and core-level spectra is often counterintuitive. For instance, systems with inhomogeneous concentration profiles can exhibit significantly larger disorder broadenings than is possible in random alloys, and even a "disorder narrowing" in some cases. For the correct interpretation of experimental spectra for complex systems, it is crucially important to understand such phenomena.

The model can be easily adapted to treat other core-level spectroscopies, the most prominent of which is Auger electron spectroscopy. Hence we expect that it should find widespread use as a framework in which to interpret experimental results. However, it is by no means a panacea. Recall that the model is underpinned by the NRA-CEFM—which itself is a particular case of the CEFM. Implicit in the NRA-CEFM are a number of approximations which may be problematic. One is the *spherical approximation*—that only the monopole moments of the charge distribution in each site are considered for the purposes of evaluating the Madelung energy. One must go beyond this approximation in order to obtain a quantitatively accurate description of the electron density within disordered alloys [44,47]. This is especially true for regions near surfaces. A generalization of the CEFM has been described in Ref. [37] which does not rely upon the spherical approximation. While the NRA-CEFM could be generalized in an analogous manner, it is not clear whether this would be fruitful. The strength of the NRA-CEFM over the "general" CEFM is its simplicity, with which comes a small loss in accuracy relative to the CEFM. It is not clear whether the gain in accuracy achieved by generalizing the NRA-CEFM to go beyond the spherical approximation is worth the resulting loss in simplicity. Another potentially problematic approximation implicit in the NRA-CEFM is that the nuclei of the system under consideration form an undistorted crystal lattice. The breakdown of this approximation can have far-reaching consequences. The addition of distortions to the crystal lattice of CuAu results in a reversal of the average relationship between a site's CLS and its number of unlike nearest neighbors [6]. The reasons for this are not known and warrant further investigation. The NRA-CEFM, suitably modified to treat lattice distortions, may add insight into this phenomenon, although it would be optimistic to expect that anything more than a qualitative understanding could be achieved.

It should be borne in mind that the aforementioned approximations, while implicit in the NRA-CEFM, are also utilized in many *ab initio* calculations and are not expected to preclude the model from making *at least* qualitatively accurate predictions. A more problematic limitation of the model is that its free parameters are not known *a priori*: they must be obtained from *ab initio* calculations or by other means. Fortunately, these parameters are highly transferable between systems; for details see Refs. [21,37]. In the future we intend to calculate these parameters for a wide range of alloys. This would enable the model to be readily applied to many systems.

ACKNOWLEDGMENT

This work was supported by the Engineering and Physical Sciences Research Council.

[1] R. J. Cole, N. J. Brooks, and P. Weightman, Phys. Rev. Lett. **78**, 3777 (1997).

[2] R. J. Cole and P. Weightman, J. Phys.: Condens. Matter **10**, 5679 (1998).

[3] D. Lewis, R. J. Cole, and P. Weightman, J. Phys.: Condens. Matter **11**, 8431 (1999).

[4] A. Newton, A. Vaughan, R. Cole, and P. Weightman, J. Electron Spectrosc. Relat. Phenom. **107**, 185 (2000).

[5] A. Newton, S. Haines, P. Weightman, and R. Cole, J. Electron Spectrosc. Relat. Phenom. **136**, 235 (2004).

[6] T. Marten, I. A. Abrikosov, W. Olovsson, B. Johansson, R. J. Cole, G. Beamson, S. R. Haines, and P. Weightman, Phys. Rev. B **79**, 012201 (2009).

[7] E. Holmström, W. Olovsson, I. A. Abrikosov, A. M. N. Niklasson, B. Johansson, M. Gorgoi, O. Karis, S. Svensson, F. Schäfers, W. Braun *et al.*, Phys. Rev. Lett. **97**, 266106 (2006).

[8] S. Granroth, R. Knut, M. Marcellini, G. Andersson, S. Svensson, O. Karis, M. Gorgoi, F. Schäfers, W. Braun, W. Eberhardt *et al.*, Phys. Rev. B **80**, 094104 (2009).

[9] G. Duscher, M. F. Chisholm, U. Alber, and M. Rühle, Nat. Mater. **3**, 621 (2004).
[10] R. Schweinfest, A. T. Paxton, and M. W. Finnis, Nature (London) **432**, 1008 (2004).
[11] M. Yamaguchi, M. Shiga, and H. Kaburaki, Science **307**, 393 (2005).
[12] H.-P. Chen, R. K. Kalia, E. Kaxiras, G. Lu, A. Nakano, K.-i. Nomura, A. C. T. van Duin, P. Vashishta, and Z. Yuan, Phys. Rev. Lett. **104**, 155502 (2010).
[13] J. Luo, H. Cheng, K. M. Asl, C. J. Kiely, and M. P. Harmer, Science **333**, 1730 (2011).
[14] J. Kang, G. C. Glatzmaier, and S.-H. Wei, Phys. Rev. Lett. **111**, 055502 (2013).
[15] D. F. van der Vliet, C. Wang, D. Tripkovic, D. Strmcnik, X. F. Zhang, M. K. Debe, R. T. Atanasoki, N. M. Markovic, and V. R. Stamenkovic, Nat. Mater. **11**, 1051 (2012).
[16] C. Chunhua, L. Gan, M. Heggen, S. Rudi, and P. Strasser, Nat. Mater. **12**, 765 (2013).
[17] W. Olovsson, E. Holmström, T. Marten, I. A. Abrikosov, and A. M. N. Niklasson, Phys. Rev. B **84**, 085431 (2011).
[18] R. J. Cole and P. Weightman, J. Phys.: Condens. Matter **9**, 5609 (1997).
[19] T. L. Underwood, P. D. Lane, N. Miller, R. Stoker, and R. J. Cole, Phys. Rev. B **79**, 024203 (2009).
[20] T. L. Underwood and R. J. Cole, J. Electron Spectrosc. Relat. Phenom. **181**, 220 (2010).
[21] T. L. Underwood and R. J. Cole, J. Phys.: Condens. Matter **25**, 435502 (2013).
[22] J. S. Faulkner, Y. Wang, and G. M. Stocks, Phys. Rev. Lett. **81**, 1905 (1998).
[23] T. Marten, W. Olovsson, S. I. Simak, and I. A. Abrikosov, Phys. Rev. B **72**, 054210 (2005).
[24] P. Soven, Phys. Rev. **156**, 809 (1967).
[25] D. D. Johnson, D. M. Nicholson, F. J. Pinski, B. L. Gyorffy, and G. M. Stocks, Phys. Rev. Lett. **56**, 2088 (1986).
[26] D. D. Johnson, D. M. Nicholson, F. J. Pinski, B. L. Györffy, and G. M. Stocks, Phys. Rev. B **41**, 9701 (1990).
[27] I. A. Abrikosov, W. Olovsson, and B. Johansson, Phys. Rev. Lett. **87**, 176403 (2001).
[28] W. Olovsson, I. Abrikosov, and B. Johansson, J. Electron Spectrosc. Relat. Phenom. **127**, 65 (2002).
[29] W. Olovsson, C. Göransson, L. V. Pourovskii, B. Johansson, and I. A. Abrikosov, Phys. Rev. B **72**, 064203 (2005).
[30] W. Olovsson, L. Bech, T. H. Andersen, Z. Li, S. V. Hoffmann, B. Johansson, I. A. Abrikosov, and J. Onsgaard, Phys. Rev. B **72**, 075444 (2005).
[31] P. Weightman and R. J. Cole, Phys. Rev. Lett. **83**, 3571 (1999).
[32] J. S. Faulkner, Y. Wang, and G. M. Stocks, Phys. Rev. Lett. **83**, 3572 (1999).
[33] M. Methfessel, V. Fiorentini, and S. Oppo, Phys. Rev. B **61**, 5229 (2000).
[34] E. Holmström, L. Nordstrom, L. Bergqvist, B. Skubic, B. Hjorvarsson, I. Abrikosov, P. Svedlindh, and O. Eriksson, Proc. Natl. Acad. Sci. USA **101**, 4742 (2004).
[35] E. Bruno, L. Zingales, and Y. Wang, Phys. Rev. Lett. **91**, 166401 (2003).
[36] V. Drchal, R. Hammerling, and P. Weinberger, Phys. Rev. B **74**, 214202 (2006).
[37] E. Bruno, F. Mammano, A. Fiorino, and E. V. Morabito, Phys. Rev. B **77**, 155108 (2008).
[38] J. S. Faulkner, Y. Wang, and G. M. Stocks, Phys. Rev. B **52**, 17106 (1995).
[39] J. S. Faulkner, Y. Wang, and G. M. Stocks, Phys. Rev. B **55**, 7492 (1997).
[40] A. V. Ruban and H. L. Skriver, Phys. Rev. B **66**, 024201 (2002).
[41] E. Bruno, Mater. Sci. Eng., A **462**, 456 (2007).
[42] B. Johansson and N. Mårtensson, Phys. Rev. B **21**, 4427 (1980).
[43] E. Bruno, L. Zingales, and A. Milici, Phys. Rev. B **66**, 245107 (2002).
[44] A. V. Ruban, S. I. Simak, P. A. Korzhavyi, and H. L. Skriver, Phys. Rev. B **66**, 024202 (2002).
[45] R. Magri, S.-H. Wei, and A. Zunger, Phys. Rev. B **42**, 11388 (1990).
[46] V. Medicherla and W. Drube, Appl. Surf. Sci. **256**, 376 (2009).
[47] F. J. Pinski, Phys. Rev. B **57**, 15140 (1998).
[48] In this work the term "Madelung interactions" is used as a synonym for "intersite Coulomb interactions."
[49] By lattice type we mean, for example, fcc, bcc, sc. Note that two lattices with the same type can have different values of R_{WS}.,
[50] A more accurate approach would be to apply "mean-field boundary conditions" beyond the nearest-neighbor shell, i.e., assume that $N_{i\mathrm{Ni}\beta} = Z_\beta c_{\mathrm{Ni}}$ for $\beta > 1$, where recall that Z_β denotes the number of sites in any site's βth nearest neighbor shell, and c_{Ni} denotes the global concentration of Ni. This would lead to better agreement between the histograms and model spectra in Fig. 1(b). However, we do not do this here for the sake of simplicity.